CHEMISTRY
A EUROPEAN JOURNAL

DOI: 10.1002/chem.200601209

Hydrogen Peroxide Decomposition by a Non-Heme Iron(III) Catalase Mimic: A DFT Study

Willi Sicking,[a] Hans-Gert Korth,[a] Georg Jansen,[a] Herbert de Groot,[b] and Reiner Sustmann*[a]

Dedicated to Professor Manfred Christl on the occasion of his 65th birthday

Abstract: Non-heme iron(III) complexes of 14-membered tetraaza macrocycles have previously been found to catalytically decompose hydrogen peroxide to water and molecular oxygen, like the native enzyme catalase. Here the mechanism of this reaction is theoretically investigated by DFT calculations at the (U)B3LYP/6-31G* level, with focus on the reactivity of the possible spin states of the Fe^{III} complexes. The computations suggest that H_2O_2 decomposition follows a homolytic route with intermediate formation of an iron(IV) oxo radical cation species ($L^{\bullet+}Fe^{IV}$=O) that resembles Compound I of natural iron porphyrin systems. Along the whole catalytic cycle, no significant energetic differences were found for the reaction proceeding on the doublet ($S=^1/_2$) or on the quartet ($S=^3/_2$) hypersurface, with the single exception of the rate-determining O–O bond cleavage of the first associated hydrogen peroxide molecule, for which reaction via the doublet state is preferred. The sextet ($S=^5/_2$) state of the Fe^{III} complexes appears to be unreactive in catalase-like reactions.

Keywords: density functional calculations · enzyme models · iron · macrocyclic ligands · N ligands

Introduction

For several years we have been interested in the mechanisms of cell injury caused by redox-active iron in combination with hydrogen peroxide.[1–4] A variety of diseases are related to oxidative cell damage, for which iron ions of the so-called labile iron pool are held responsible.[5–7] Living systems have developed strategies by which the noxious action of redox-active iron(II)/(III) can be counteracted. Among them, hydrogen peroxide, a ubiquitous metabolite in living cells, is converted to water and oxygen by the family of catalase enzymes[8–10] to avoid production of cell-damaging hydroxyl radicals via reaction with Fe^{II} ions (Fenton reaction). Catalase degrades hydrogen peroxide according to the stoichiometry of Equation (1) and thereby regulates the concentration of hydrogen peroxide to physiological levels.

$$2\,H_2O_2 \rightarrow 2\,H_2O + O_2 \qquad (1)$$

The production of oxygen and water from the decomposition of two molecules of hydrogen peroxide by catalase is a multistep reaction with an iron(IV) oxo porphyrin radical cation (por$^{\bullet+}$Fe^{IV}=O, Compound I) as a key intermediate.[8–11] Compound I species, which vary in the proximal axial ligand, are commonly accepted as intermediates in oxygenation reactions catalyzed by a variety of other heme enzymes, for example, peroxidases[12] and cytochromes P450.[13] The crucial mechanistic step in formation of Compound I is generally believed to be an ionic, nonradical step in which an intermediate hydroperoxyl (HOO^-) Fe^{III} porphyrin complex is protonated at the hydroperoxide OH group with spontaneous elimination of water. In native enzymes, including catalase, this protonation step is facilitated by a distal histidine residue which acts as a general acid–base catalyst. (Homolytic O–O bond cleavage of the hydro-

[a] Dipl.-Ing. W. Sicking, Dr. H.-G. Korth, Prof. Dr. G. Jansen, Prof. Dr. R. Sustmann
Institut für Organische Chemie
Universität Duisburg-Essen, Campus Essen
Universitätsstrasse 5, 45117 Essen (Germany)
Fax: (+49) 201-183-4259
E-mail: reiner.sustmann@uni-duisburg-essen.de

[b] Prof. Dr. H. de Groot
Institut für Physiologische Chemie
Universitätsklinikum Essen
Hufelandstrasse 55, 45122 Essen (Germany)

Supporting information for this article is available on the WWW under http://www.chemeurj.org/ or from the author.

peroxyl ligand, on the other hand, would lead to formation of Compound II (porFe^{IV}=O), the product of one-electron reduction of Compound I).

In recent years, numerous computational studies were published in which the mechanisms of formation of Compound I-type ferryl oxo species and their role in heme- and non-heme-catalyzed oxygenations have been investigated.[14–24] However, the detailed mechanisms of such reactions are still a matter of debate. Noteworthily, ferryl oxo intermediates have recently been produced also from non-heme iron complexes.[25–28] Their spectroscopic properties clearly show that they are structurally and electronically very similar to Compound I, and this highlights their key role in oxygenations mediated by iron complexes.

Low molecular weight, membrane-permeable mimics of catalase may enhance and support the innocuous decomposition of hydrogen peroxide, either in cases of pathological concentrations of Fe$^{II/III}$ or where the hydrogen peroxide concentration must be regulated. In recent years, we have been interested in the development of such catalase mimics based on macrocyclic non-heme Fe^{III} complexes, and we presented **1** (Scheme 1), the first enzyme mimic of catalase

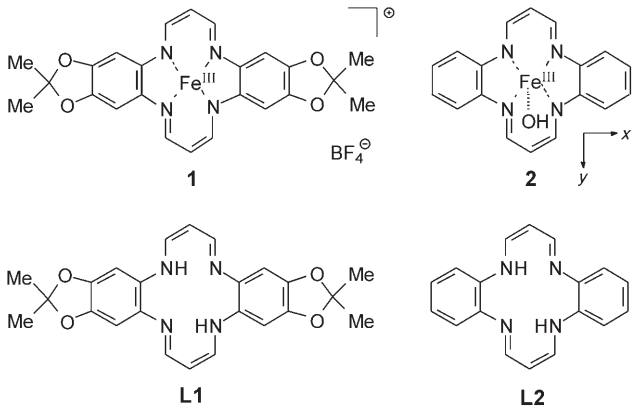

Scheme 1. Fourteen-membered tetraaza macrocycles and related Fe^{III} complexes as catalase mimics.

which, as the tetrafluoroborate or chloride salt, acts under truly "physiological" conditions, that is, at ambient temperature and at low concentrations (micromolar) of H_2O_2 and catalyst in aqueous solution at a pH of around 7.[29] Complex **1** decomposes hydrogen peroxide according to the catalase stoichiometry [Eq. (1)]. Recently, it was also shown that not only iron(III) complex **1**, but also its free ligand **L1** protects cells against oxidative damage.[4] The positive antioxidative effect of **L1** has been attributed to the capability of the ligand to penetrate cell membranes (as proven by ESI-MS), as well as intracellular formation of a catalase-active iron complex in situ by binding of free, redox-active iron.

In previous work, a variety of Fe^{III} complexes analogous to **1**, that is, having a [N_4] bonding motif similar to those of porphyrins, have been prepared and tested for their catalase-like activity.[30] Mössbauer spectroscopy and susceptibility measurements revealed that in the solid state the Fe^{III} center of the catalytically active preparations of the five-coordinate complexes of type **1** resides in the intermediate ($S=^3/_2$) spin state. Related high-spin ($S=^5/_2$) complexes turned out to be inert with respect to H_2O_2 decomposition.

In addition to ongoing experimental studies on the mechanism by which the above catalase mimics decompose hydrogen peroxide, we studied the mechanism also by quantum-chemical calculations utilizing density functional theory (DFT). Here, we present our first results. Shortly after our first report on the catalase-like activity of **1**, a theoretical analysis of the possible mechanism by DFT calculations was published.[31] This study, however, suffered seriously from the restriction of using the bare, positively charged tetracoordinate Fe^{III} complex of ligand **L1** as a model, that is, no additional axial (proximal) ligand was taken into account. The computations then predicted that such an Fe^{III} **L1** complex should not exist, but rather provided a Fe^{II} complex of the oxidized, radical cationic form of ligand **L1**, that is, an electron has been transferred from the ligand to the iron center. We obtained the same result for the Fe^{III} complex of the unsubstituted ligand **L2** (data not shown). This outcome, of course, is a consequence of the square-planar coordination, which prefers Fe^{II} in the low-spin state. Furthermore, in buffered aqueous solution the complex must be expected to be hexacoordinate, with two molecules of water occupying the axial positions or even complexed by water and a negatively charged ligand such as OH^- or any other of the anions present in solution. Thus, restriction of the calculations to an [N_4] tetracoordinate complex is an oversimplification which may lead to mechanistically misleading results.

The present investigation is based on the structural characteristics of catalase.[9,10] In native iron catalases, the fifth (proximal) coordination site of the prosthetic heme group is occupied by the phenolate anion of a tyrosine residue; the sixth, distal coordination site is empty in the resting state of the enzyme and is the site of coordination by hydrogen peroxide during the catalytic cycle. In the present computational study we employed unsubstituted ligand **L2** as a model for **L1** to reduce the computational effort. This is justified because it was found that the Fe^{III} complex of ligand **L2** (as the chloride salt) exhibits catalase-like activity in aqueous buffer at pH 7 similar to that of **1**.[30] We therefore selected Fe^{III} complex **2** as a model in which a hydroxide anion occupies the proximal coordination site and thereby renders the complex uncharged. Besides mimicking the tyrosinate of native catalase,[32] coordination of a hydroxide ion seems to be realistic with respect to the observed catalytic action of **1**. It is well known that coordination to Fe^{III} increases the acidity of water molecules dramatically;[33,34] hence, it is very likely that in aqueous buffer at pH 7 a coordinated water molecule will be (partially) deprotonated. Of special importance for the reactivity of Fe^{III} complexes is the spin state of the iron center.[20,21] Hexacoordinate Fe^{III} prefers the low-spin, doublet ($S=^1/_2$), state in strong octahedral fields, whereas pentacoordinate Fe^{III} exists primarily in the high-spin, sextet state ($S=^5/_2$),[35,36] but some intermediate, quar-

tet-state ($S=^3/_2$) complexes are also known.[37–42] Therefore, special attention will be paid to the reactivity of the different spin states. Experimentally, decomposition of H_2O_2 has been performed in aqueous solution, whereas the computations refer to gas-phase processes. Since solvation (bulk polarity) effects can be very important, especially for spin-state ordering, the energies of the starting complexes, the transition states for the first, rate-limiting step of H_2O_2 decomposition, and the intermediate ferryl oxo species were also computed for aqueous solution by employing the CPCM continuum solvation model.

Computational Details

Density functional calculations were carried out with the Gaussian 03 suite of programs.[43] All open-shell structures were calculated at the UB3LYP/6-31G* level of theory; for closed-shell molecules B3LYP/6-31G* was employed. A few small compounds were additionally calculated by the CBS-QB3 complete basis set approach.[44] The iron complexes were individually optimized for their different spin multiplicities. The effect of diffuse functions and core potentials for Fe on the relative energies of the spin states were tested for a limited number of compounds by single-point UB3LYP/6-31+G(d), LanL2DZ(Fe)+UB3LYP/6-31G(d), and SDD(Fe)+UB3LYP/6-31G(d) calculations. Below, the spin multiplicities of the iron complexes are indicated by a left-hand superscript. Ground or transition state properties were established by frequency calculations; the energies given below are corrected for zero-point vibrational energy (ZPVE). ZPVEs were scaled by a scaling factor of 0.9806. Starting orbitals of structures with three unpaired electrons were generated by a quartet single-point calculation, that is, these orbitals were also taken as starting orbitals for the computation of the doublet state. This provided electron distributions of lowest energy. For all structures the stability of the wave function was checked by a pre-calculation with the keyword STABLE; in case of initial instability, stable wave functions were generated with STABLE=OPT. For a few structures (see below) the effect of aqueous solvation was analyzed by performing single-point calculations with the CPCM polarizable continuum solvation model incorporated in Gaussian. Total energies and coordinates of optimized structures are given as Supporting Information.

Results and Discussion

Spin states of Fe^{III} complexes 2: Geometry optimizations were carried out for three possible electronic configurations of **2**—doublet (low-spin, $S=^1/_2$, ^{2}**2**), quartet (intermediate-spin, $S=^3/_2$, ^{4}**2**), and sextet (high-spin, $S=^5/_2$, ^{6}**2**)—although in reality a doublet ($S=^1/_2$) spin state of **2** appears to be rather artificial for a five-coordinate Fe^{III} complex. Optimized structures and related spin densities are displayed in Figure 1. In the spin density distributions, shown below the related molecular structures, the size of the circle at a given center directly corresponds to the magnitude of the spin density, and dark gray and light gray shading indicate positive and negative spin, respectively. For the macrocyclic ligand, the numerical value is the algebraic sum over all atoms. Relative energies were calculated with respect to the energy of intermediate-spin complex ^{4}**2** (plus the energies of H_2O_2 and/or H_2O), because the $S=^3/_2$ spin state was found experimentally for the catalytically active complex in the solid state.[30] Relative energies are collected in Table 1; relative, zero-point-corrected electronic energies at 0 K are also displayed in Figure 2; graphical schemes of the relative enthalpies and Gibbs free energies, respectively, are provided in Figures S1 and S2 in the Supporting Information.

The high-spin structure ^{6}**2** was found to be the lowest energy complex, marginally stabilized, by 0.6 kcal mol^{-1} compared to the intermediate-spin complex ^{4}**2**. The low-spin structure ^{2}**2** is destabilized by about 3.2 kcal mol^{-1}. As the total energy of complexes ^{2}**2**–^{6}**2** might to some extent be dependent on the relative rotational orientation of the proxi-

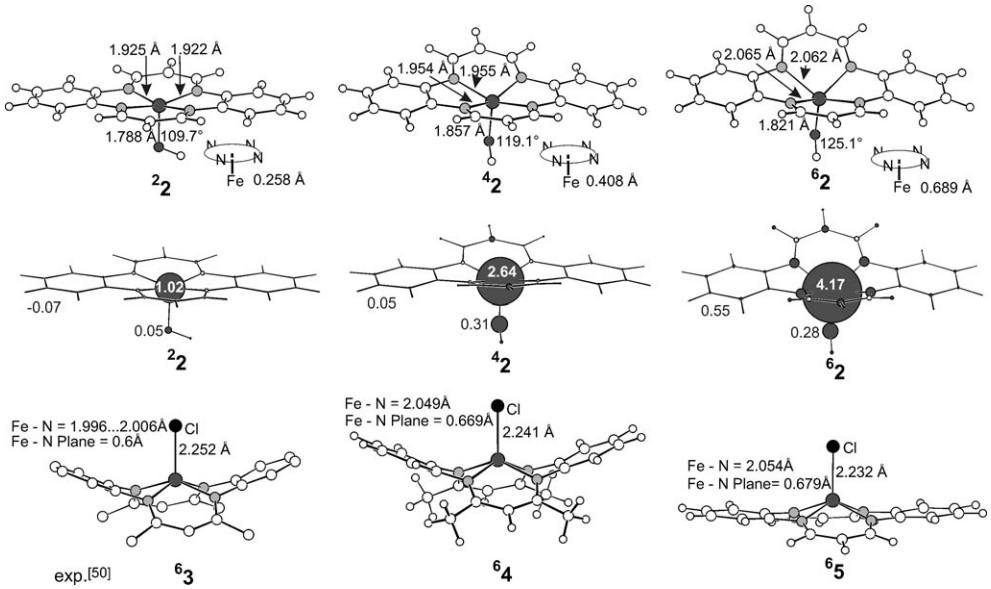

Figure 1. Calculated structures (top) and spin densities (middle) of pentacoordinate complexes **2** and experimental (hydrogen atoms omitted)[50] and calculated structures of high-spin chloride complexes **3**–**5** (bottom).

Table 1. Relative UB3LYP/6-31G* energies [kcal mol^{-1}] for reaction of Fe^{III} complex **2** with H_2O_2.[a]

Compound	ΔE^0	$\Delta(E^0+ZPVE)$	ΔH^{298K}	ΔG^{298K}	ΔE^0_{SCRF}[b]	$\Delta(E^0_{SCRF}+ZPVE)$[b]
^{2}**2**$+H_2O_2$	2.15	3.2	2.9	3.6	2.18	3.2
^{4}**2**$+H_2O_2$	**0.0**	**0.0**	**0.0**	**0.0**	**0.0**	**0.0**
^{6}**2**$+H_2O_2$	0.32	−0.6	−0.3	−1.2	2.34	1.5
^{4}**2**$+H_2O$	**(0.0)**	**(0.0)**	**(0.0)**	**(0.0)**	**(0.0)**	**(0.0)**
^{2}**6**[c]	−8.03	−4.8	−5.7	5.2	−4.73	−1.5
^{4}**6**[c]	−5.02	−3.9	−3.7	3.8	−1.00	0.2
^{6}**6**[c]	−4.69	−4.4	−3.9	3.1	1.75	1.9
^{2}**7a**	−6.88	−4.2	−4.8	7.5	0.39	3.1
^{2}**7b**	−6.89	−4.2	−4.8	7.3	1.18	3.9
^{4}**7**	−5.60	−4.5	−4.2	4.6	1.90	3.0
^{6}**7**	−5.49	−5.3	−4.7	3.4	4.02	4.2
^{2}**8a**	5.93	6.4	5.7	18.0	12.06	12.5
^{2}**8b**	7.61	7.8	7.2	19.8	12.88	13.1
^{4}**8**	14.22	13.7	-13.5	24.4	19.54	19.0
^{1}**9** + $^{\bullet}$OH	14.91	12.5	12.8	15.2		
^{3}**9** + $^{\bullet}$OH	8.68	6.7	7.0	9.3		
^{5}**9** + $^{\bullet}$OH	30.41	26.0	26.8	28.0		
^{2}**10**	−7.93	−7.4	−8.1	5.4		
^{4}**10**	−7.88	−7.3	−8.0	5.2		
^{2}**11**	−6.50	−8.5	−9.5	4.6		
^{4}**11**	−6.87	−8.4	−9.7	4.1		
^{2}**12**	−24.18	−23.6	−23.5	−13.4		
^{4}**12**	−24.28	−23.5	−23.5	−13.7		
^{6}**12**	−6.28	−7.2	−6.7	2.2		
^{2}**13**$+H_2O$	−12.63	−13.9	−13.4	−12.0	−18.24	−19.5
^{4}**13**$+H_2O$	−12.76	−13.8	−13.5	−12.3	−18.19	−19.3
^{6}**13**$+H_2O$	4.60	1.8	2.6	2.7	0.82	−2.0
^{4}**20**	−4.87	−4.1	−4.6	7.6		
^{2}**21**	−50.05	−46.3	−47.9	−32.4		
^{4}**21**	−31.89	−30.4	−31.2	−18.0		

[a] Energies are given relative to ^{4}**2**$+H_2O_2$ unless otherwise noted. [b] SCRF energies for aqueous solution from CPCM solvation model. [c] Energies relative to ^{4}**2**$+H_2O$.

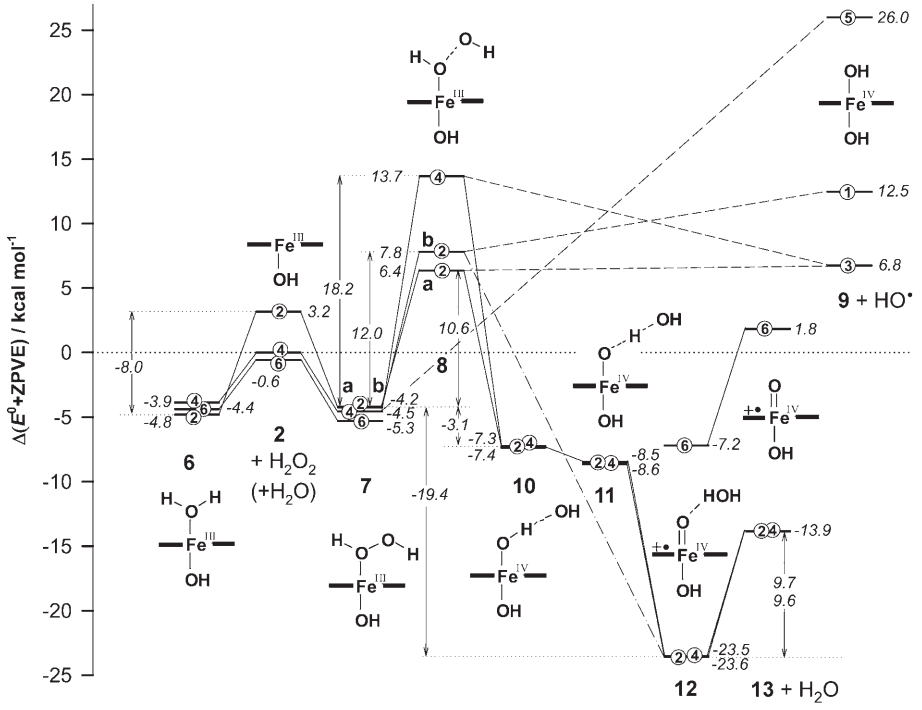

Figure 2. Energy (0 K) scheme for reaction of Fe^{III} complexes **2** with hydrogen peroxide. Encircled numbers denote the spin multiplicities; the macrocyclic ligand is symbolized by solid horizontal bars.

mal hydroxide ligand, we pinpointed the lowest energy rotamers by starting the geometry optimizations from various initial rotational orientations of the OH group. In ^{2}**2**, the O–H bond is aligned along the *x* axis, which bisects the phenylene groups of the macrocycle (see Scheme 1). No other stable rotamer could be found. The orthogonal orientation, along the *y* axis bisecting the *meso*-carbon atoms represents a rotational transition structure 5.5 kcal mol^{-1} higher in energy. In contrast, the latter orientation is found for the lowest energy ground-state structures of ^{4}**2** and ^{6}**2**, for which the orthogonal orientations along the *x* axis are first-order saddle points. The barriers for OH rotation, however, are rather low (0.8 and 0.4 kcal mol^{-1}, respectively).

The macrocyclic ligand of complex ^{2}**2** is nearly planar with the iron(III) ion displaced by only 0.26 Å toward the hydroxide ligand out of the plane defined by the four nitrogen atoms of the macrocycle. The macrocycle shows a slight saddlelike deformation with outward bending of the propylidene units away from the OH binding side. The iron–nitrogen bond lengths are about 1.922 Å, and the iron–oxygen bond length is 1.788 Å. The displacement by 0.26 Å on attachment of the axial hydroxide group may be related to increased orbital overlap between the macrocycle orbitals and the Fe–O orbitals[45] because removal of this group leads to a perfectly planar structure of the corresponding tetracoordinate complex (not shown). In complex ^{4}**2** with quartet spin state, the metal ion resides 0.41 Å above the plane of the four nitrogen atoms and the macrocyclic ligand assumes a distinctly saddlelike structure. The iron–

nitrogen bond lengths of 1.955 Å are similar to those in ^{2}**2**, but the iron–oxygen bond is elongated to 1.857 Å. An even more pronounced saddlelike deformation is found in high-spin complex ^{6}**2**. Here, the iron atom resides 0.69 Å above the reference plane; the iron–oxygen bond length (1.821 Å) is slightly increased compared to that in ^{2}**2** (1.788 Å), but shorter than that in ^{4}**2** (1.857 Å). The energetic preference for a high-spin, square-pyramidal structure is in line with the resting Fe^{III} state of native catalases (ferricatalase).[46,47]

Noteworthily, the predicted energy differences of the spin states of our complexes are strikingly similar to what has been computed, at a similar theoretical level, for pentacoordinate Fe^{III} porphyrin thiolate complexes, that is, modeling the mechanisms of cytochrome P450 monooxygenase.[21,48] For such complexes the doublet state was found to be 4.1–4.3 kcal mol^{-1} less stable than the sextet state. Differently to our system, however, Shaik et al.[21] reported destabilization of the corresponding quartet state by the same amount, whereas Guallar and Friesner[48] found only a minor difference between the quartet and sextet states. The energetic order seems to be a manifestation of the different degree of out-of-plane dislocation of the iron center in the quartet state relative to the doublet state, which is only 0.04 Å for the complexes of Shaik et al. but 0.15 Å for our structures (see Figure 1).

The spin density in complexes **2** (Figure 1) is mainly located on iron: $\rho_{Fe}=1.02$ in low-spin complex ^{2}**2** and $\rho_{Fe}=2.64$ in intermediate-spin complex ^{4}**2**. In the latter, a spin density of $\rho_{O}=0.29$ is found on the hydroxyl oxygen atom. In both cases almost no unpaired spin density is transferred to the macrocyclic ligand. This is different in the high-spin structure ^{6}**2**, where due to the strongly ruffled structure the ligand π orbitals may significantly mix with the iron d_{z^2} orbital,[49] providing a spin density of $\rho_{Fe}=4.17$ on iron and of $\rho_{O}=0.29$ on the hydroxyl oxygen atom. Sizeable spin delocalization on the macrocyclic ligand is indicated by a total spin density of $\rho_{L}=0.54$, mainly concentrated on the four nitrogen atoms. This spin distribution is surprisingly close to those computed for five-coordinate high-spin Fe^{III} porphyrin complexes.[49]

How reliable can the computed structures of the Fe^{III} complexes be considered? In 1976 Weiss and Goedken[50] published an X-ray structure of the high-spin ($S=^{5}/_{2}$) Fe^{III} chlorido complex ^{6}**3** (Figure 1, hydrogen atoms omitted), the tetramethyl-substituted derivative of ligand **L2**. The experimental structure is largely reproduced by the UB3LYP/6-31G* optimized structure of ^{6}**4**, as is evident from the bond lengths and the out-of-plane displacement of the iron(III) ion (0.67 Å). The influence of the methyl groups on the geometry of the macrocyclic ligand is revealed by comparison with the calculated structure of chlorido complex ^{6}**5** where the four methyl groups are omitted. The saddle-shaped distortion of the macrocycle is strongly reduced compared to ^{6}**4**, but the displacement of the iron center (0.68 Å) remains virtually unchanged. Thus, a major fraction of the saddlelike distortion of the ligand in ^{6}**3** and ^{6}**4** is induced by steric interactions of the four methyl groups. This is confirmed by the computed structures of the corresponding iron-free ligands, which are perfectly planar (not shown). We further observe that the pertinent geometrical parameters of complexes **2** compare nicely to those of five-coordinate Fe^{III} porphyrins.[35,49] Thus, the UB3LYP/6-31G* procedure can be assumed to provide reliable structures for these complexes.

Water adducts of Fe^{III} complexes 2: In terms of their catalase-like activity, the pentacoordinate Fe^{III} complexes ^{2}**2**–^{6}**2** are unlikely to represent the actual "resting state" of catalyst **2** in aqueous solution. Rather, in aqueous solution the complexes are expected to be hexacoordinate, ligated by a distal water molecule. This, however, might alter the relative stability of the three spin states, and this is indeed the case. The computations predict that the three spin states of aquo complexes **6** (Figure 3) are very close in energy, differing by only 1 kcal mol^{-1} (Table 1, Figure 2). Thus, coordination of water leads to energetic stabilization relative to parent complexes **2** by -3.9 kcal mol^{-1} for ^{4}**6** and ^{6}**6**, but by -8.0 kcal mol^{-1} for ^{2}**6**, so that the latter is just rendered the most stable structure. This again nicely parallels the findings from theoretical studies on P450 enzymes,[21,48] which indicate that a distal water ligand favors the doublet spin state of the enzyme's resting state. The short Fe–OH_2 distance of 2.214 Å and the small out-of-plane displacement of 0.12 Å of the iron(III) ion reflects essentially octahedral coordination of ^{2}**6**. Here, the water hydrogen atoms individually display OH–π contacts (both 2.531 Å) to two adjacent nitrogen atoms of the macrocycle. On the other hand, the long Fe–OH_2 distances of 3.588 and 3.895 Å in ^{4}**6** and ^{6}**6**, respectively, suggest that these structures should rather be regarded as van der Waals complexes of pentacoordinate iron(III), because the square-pyramidal structure of the parent complexes ^{4}**2** and ^{6}**2** with a strongly ruffled macrocycle remains essentially unchanged. In both ^{4}**6** and ^{6}**6**, the two water hydrogen atoms display a weak, bifurcated OH–π contact to the same nitrogen atom (^{4}**6**: 2.846 and 2.916 Å; ^{6}**6**: 2.817 and 2.983 Å) which induces some displacement (13–14°) of the water ligand away from the vertical z axis. With regard to the spin state that is actually responsible for the catalase activity of the complexes, the energetic similarity of the spin states opens the possibility that complexes ^{2}**6**, ^{4}**6**, and ^{6}**6** might exist in thermal equilibrium in aqueous solution at room temperature (see below).

In accord, when aqueous solvation was taken into account by means of the CPCM solvation model, the overall picture did not change much (Table 1 and Figure S3 in the Supporting Information). The parent, pentacoordinate, quartet-state complex ^{4}**2** now turned out to be the most stable structure, lying 1.5 and 3.2 kcal mol^{-1} below the sextet and the doublet states, respectively. Addition of water again induced the greatest stabilization for the doublet state (^{2}**6**), whereas the other two states were only marginally affected. The general stabilization effect on structures **2** by complexation of water, however, was 3.3–6.2 kcal mol^{-1} smaller than computed for the gas phase.

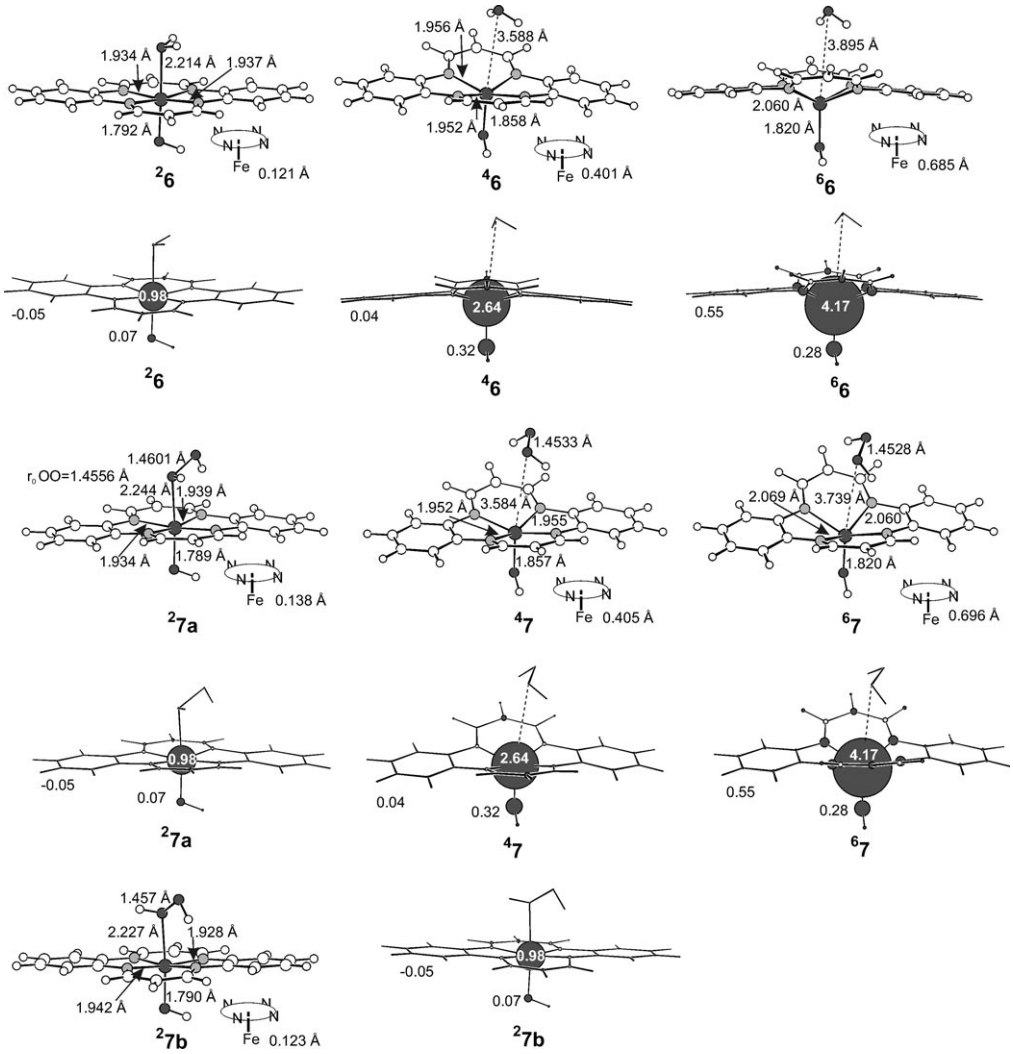

Figure 3. Calculated structures and spin densities of complexes **6** and **7**.

Hydrogen peroxide adducts of Fe^{III} complexes 2: The hydrogen peroxide complexes **7** are structurally very similar to the aqua complexes **6** (Figure 3). In all three spin states, H_2O_2 coordinates "end-on" to the iron center. For the doublet state, two energetically almost identical conformers with respect to the arrangement of the axial H_2O_2 ligand, ^{2}**7a**, ^{2}**7b**, were found. In these structures, the Fe^{III} ion is displaced by 0.12 and 0.13 Å, respectively, toward the proximal hydroxide ligand, similar to the displacement in the aqua complex ^{2}**6**. The Fe–O_2H_2 distances are 2.244 (^{2}**7a**) and 2.227 Å (^{2}**7b**). The adducts appear to be further stabilized by OH–π interactions with the negatively charged nitrogen atoms of the ligand π system. (For the sake of simplicity, hydrogen contacts to the π system of the macrocycle will henceforth also be termed "hydrogen bonds"). In ^{2}**7a** both hydrogen atoms of the peroxide are singly hydrogen bonded ($r_{\text{outer H}}=2.053$, $r_{\text{inner H}}=2.595$ Å) to the adjacent nitrogen atoms of one diaminopropylidene unit of the macrocycle. In ^{2}**7b** the "inner" hydrogen atom of H_2O_2 points in the direction of a *meso*-carbon atom and thus forms a bifurcated hydrogen bond ($r=2.681$ and 2.704 Å) to the geminal nitrogen atoms of a diaminopropylidene unit. The terminal hydrogen atom is singly hydrogen bonded ($r=2.074$ Å) to a third nitrogen atom. Interestingly, these arrangements allow the associated hydrogen peroxide to largely retain its ground state (gas-phase) conformation, as is evident from comparison with the experimental and B3LYP/6-31G* and CBS-QB3-calculated data (Table 2). The O–O bond lengths are only slightly longer (1.457 and 1.460 Å, respectively) than the experimental gas-phase value (1.4556 Å[51]), and this indicates only minor weakening of the bond. Complexes ^{2}**7** are stabilized by -7.4 kcal mol^{-1} with respect to isolated ^{2}**2**$+H_2O_2$, somewhat less (0.6 kcal mol^{-1}) than water complex ^{2}**6** (Table 1 and Figure 2).

The hydrogen peroxide adducts of quartet and sextet states, ^{4}**7** and ^{6}**7**, display long Fe–O_2H_2 distances of 3.584 and 3.739 Å, respectively, like in the related water complexes ^{4}**6** and ^{6}**6**. Also, the displacement of the iron(III) ion towards the hydroxyl group remains essentially the same. In both complexes, the O–O bond length of the coordinated

Table 2. *cis* rotational barrier and geometrical parameters of H_2O_2 in the ground state (GS), in the transition state for rotation (TS), and in Fe^{III} complexes **7**, **14a**, and **14b**.[a]

Compound	E_{rot} [kcal mol^{-1}]	r(O–O) [Å]	r(O–H) [Å]	r(O–H)[b] [Å]	O-O-H angle [°]	O-O-H angle[b] [°]	Dihedral angle [°]
H_2O_2 GS		1.4556	0.974		99.7		118.5
H_2O_2 GS[c]		1.4537	0.966		100.1		120.3
H_2O_2 GS[d]		1.4556	0.967		102.3		113.7
		1.4645	0.965		99.4		111.8
H_2O_2 TS	8.4[e]	1.4653	0.974		104.7		0.0
H_2O_2 TS[c]	7.1[e]	1.4616	0.966		104.9		0.0
^{2}**7a**		1.4601	0.982	0.976	98.2	100.5	124.7
^{2}**7b**		1.4573	0.982	0.975	98.5	101.0	115.4
^{4}**7**		1.4533	0.977	0.975	100.4	100.6	103.7
^{6}**7**		1.4528	0.976	0.976	100.5	100.7	100.2
^{2}**14a**		1.4531	0.974	0.997	100.1	100.7	98.2
^{4}**14a**		1.4531	0.974	0.997	100.1	100.7	98.7
^{2}**14b**		1.4678	0.985	0.986	99.4	99.2	7.0
^{4}**14b**		1.4679	0.985	0.986	99.4	99.3	5.0

[a] B3LYP/6-31G*//B3LYP/6-31G* unless otherwise noted. [b] OH nearest to Fe. [c] CBS-QB3. [d] Experimental data.[51,65] [e] Experimental values: 7.11,[65] 7.33 kcal mol^{-1}.[64]

hydrogen peroxide (1.453 Å) corresponds to that of the isolated molecule; the HOOH dihedral angles (104 and 100°) are somewhat reduced compared to that in ^{2}**7a,b** or in free hydrogen peroxide (Table 2). In contrast to ^{2}**7a,b**, the binding of H_2O_2 in ^{4}**7** and ^{6}**7** (-4.5 and -4.7 kcal mol^{-1}, respectively, versus parent **2**) is slightly stronger than the binding of water in ^{4}**6** and ^{6}**6**, respectively. The stronger binding of H_2O or H_2O_2 in the doublet state parallels native catalase, in which the high-spin resting state changes to low-spin on coordination of hydrogen peroxide as the sixth ligand.[10] The spin densities on iron of all spin states of **7** are identical to those in the aquo complexes **6** (Figure 3).

It is evident from Table 1 and Figure 3 that the stronger binding of H_2O or H_2O_2 to complex **2** in its low-spin state (^{2}**2**) than in its intermediate- (^{4}**2**) or high-spin state (^{6}**2**) compensates the higher intrinsic stability of the last two. This fact suggests that the actual geometry in aqueous solution and hence the spin state(s) required for hydrogen peroxide decomposition might be achieved by equilibration, irrespective of the structure and spin state of the parent solid complex. This view is supported by calculations of the energy of the H_2O_2 adducts **7** as a function of the Fe–O_2H_2 distance (see Figure S4 in the Supporting Information). Successive decrease of the Fe–O_2H_2 distance below the fully optimized equilibrium structure and reoptimization of all other structural parameters results in reduced bonding energy until, at Fe–O distances of 2.2 and 2.5 Å, the Fe^{III}–H_2O_2 interaction in the quartet (^{4}**7**) and sextet states (^{6}**7**), respectively, become repulsive, that is, at distances close to the equilibrium distance (2.227/2.244 Å) of the doublet-state structures ^{2}**7a,b**. The doublet state becomes repulsive at a significantly shorter distance of 1.8 Å. The quartet and sextet potential curves cross the doublet potential curve already at 2.8 and 3.2 Å, respectively; hence, at these distances $S=3/2 \rightleftharpoons S=1/2$ or $S=5/2 \rightleftharpoons S=1/2$ spin-state interconversion may take place with low estimated barriers of 2–3 kcal mol^{-1}.

Inclusion of aqueous solvation (Table 1, Figure S3 in the Supporting Information) predicted only a negligible (<0.7 kcal mol^{-1}) change in energy on association of H_2O_2 with ^{2}**2**, but destabilization of the H_2O_2 complexes ^{4,6}**7** by 3.0 and 4.2 kcal mol^{-1} versus the parent components ^{4,6}**2** + H_2O_2, respectively, that is, replacement of H_2O in complexes **6** by H_2O_2 is 2.8–5.4 kcal mol^{-1} uphill. Nevertheless, since structures **7** again are essentially degenerate, rapid spin-state equilibration should also take place in aqueous solution.

Formation of ferryl oxo (Fe^{IV}=O) intermediates: In native enzymes, including catalase, formation of Compound I is facilitated by a distal histidine residue which acts as a general acid–base catalyst. However, formation of Compound I has also been proposed for enzymes which lack such a strategically positioned acid–base catalyst (e.g., $P450_{cam}$).[48,52] In such cases, a water molecule in the enzyme pocket has been proposed to contribute to the protonation step.[48] This has been questioned, because it has been found that the terminal oxygen atom of the hydroperoxyl ligand of Fe^{III} porphyrins has a much lower (by 30–40 kcal mol^{-1}) proton affinity than the iron-bound ("inner") oxygen atom,[52] and thus protonation at the latter position to give a neutral H_2O_2 ligand is strongly favored. Furthermore, protonation of the inner oxygen atom of the hydroperoxide group has been found to strongly lower the barrier for O–O bond homolysis.[24,52–54] In accord, it has been observed that O–O bond cleavage is rate-limiting in some reactions, which would indicate participation of a neutral H_2O_2 adduct.[55] Recently, measurements of kinetic isotope effects provided further evidence that a properly located histidine residue is necessary to enforce the ionic mechanism of Compound I formation, whereas in its absence a radical process might be feasible.[56]

Since the latter situation holds for our catalysts, we therefore have good reason to believe that H_2O_2 decomposition follows a homolytic path in our case. To model the next stage of the catalytic reaction, the O–O bond length of coordinated H_2O_2 in complexes **7** was taken as the reaction coordinate. By this means, transition states (TS) for O–O bond cleavage (**8**) on the doublet and quartet hypersurface could be located, but not for the sextet ($S=5/2$) state (Figure 4). In the last-named case, on transition-state search the energy always increased continuously towards dissociation into the quintet-state ($S=2$) dihydroxy complex ^{5}**9** and free HO$^\bullet$ (31.3 kcal mol^{-1} above ^{6}**7**; Figure 2, Table 1) without converging to a first-order saddle point. Hence, it appears highly unlikely that H_2O_2 decomposition proceeds on the sextet hypersurface, and the sextet-state route was not further pursued. Interestingly, on the doublet surface two transition states, ^{2}**8a** and ^{2}**8b**, were found in geometry optimiza-

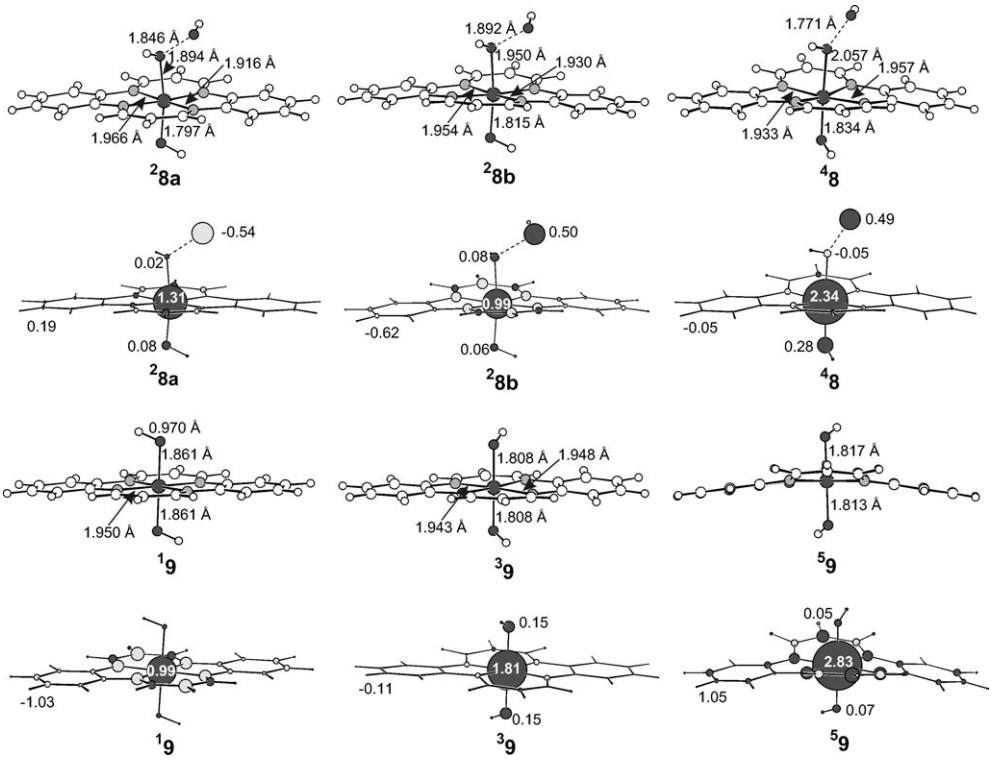

Figure 4. Calculated structures and spin densities of complexes **8** and **9**.

tions starting from the two stable arrangements of the associated hydrogen peroxide (**^{2}7a** and **^{2}7b**, respectively). The two doublet transition states **^{2}8a**,**b** differ in energy by about 1.4 kcal mol^{-1} and are characterized by different distributions of the unpaired spin density (see below). In **^{2}8a**, the O–O bond is stretched to 1.846 Å, and the Fe–O(H)OH bond shortened to 1.894 Å, while in **^{2}8b** these values are 1.892 and 1.950 Å, respectively (Figure 4). Remarkably, on the $S=^3/_2$ surface, shortening of the Fe–O(H)OH distance is much stronger, from 3.584 in **^{4}7** to 2.057 Å in TS **^{4}8**. This indicates much stronger bonding of the H_2O_2 unit on elongation of the O–O bond (1.771 Å). Frequency and spin-density analysis confirmed that in fact the three transition structures all represent a possible barrier for homolytic O–O bond cleavage. The lowest barrier is predicted for **^{2}8a**, which lies just 10.6 kcal mol^{-1} above precursor complex **^{2}7a**, followed by **^{2}8b** at 12.0 kcal mol^{-1} above **^{2}7b** (Figure 2). The quartet-state barrier **^{4}8** lies significantly higher, 18.2 kcal mol^{-1} above **^{4}7**.

Since the rate-limiting bond-breaking step **7**→**8** appeared to be crucial with respect to spin-state dependence (see below), we checked whether basis sets or aqueous solvation significantly influence the energies and ordering of the spin states of these structures. As is evident from the data of Tables S2 and S3 in the Supporting Information, inclusion of diffuse functions [B3LYP/6-31+G(d)] or using common basis sets which include core potentials for iron (LanL2DZ, SDD; all other atoms B3LYP/6-31G*) does not change the general picture. In all cases, the energies of complexes **^{2}7a** and **^{2}7b** are almost the same (within 0.4 kcal mol^{-1}) in the gas phase; in aqueous solution they differ by 1.3 kcal mol^{-1} at most. Inclusion of diffuse functions inverts the relative ordering of TSs **^{2}8a** and **^{2}8b**, but not that of the doublet and quartet states. The barrier heights are somewhat reduced, by −0.2 and −1.7 kcal mol^{-1} for **^{2}8a** and **^{2}8b**, respectively, but slightly increased (+0.4 kcal mol^{-1}) for **^{4}8**. The core-potential basis sets uniformly predict barriers that are about 1–5 kcal mol^{-1} higher than the all-electron basis sets, but again the quartet state TS **^{4}8** lies significantly (9–10 kcal mol^{-1}) higher than the doublet states. Noteworthily, the doublet-state barrier for O–O bond homolysis in the H_2O_2 complex of a P450 model (porphine thiolate) has been computed (B3LYP/LACVP) to be in the range 16.3–19.2 kcal mol^{-1},[24] that is, quite similar to our data.

Considering aqueous solvation, the CPCM model predicts that **^{2}7a** should be the preferred ground-state structure in aqueous solution, and all barriers are lower by 0.6–4 kcal mol^{-1} than in the gas phase. However, the relative spin-state ordering is preserved in aqueous solution, irrespective of the basis set. Hence, the calculations suggest that (the kinetics of) the first stage of the catalytic reaction, O–O bond homolysis, is controlled by spin state and preferably proceeds by the doublet-state route.

As is evident from the data presented below, the **^{2}7a**,**b**→**^{2}8a**,**b** barrier turned out to be the rate-limiting step for the whole catalytic cycle. The related gas-phase Gibbs free energies of activation were computed as $\Delta G^{\neq}=10.5/12.5$ kcal mol^{-1} (Table 1, see Figure S2 in the Supporting Informa-

tion). These can be compared with the experimental Gibbs free energies of activation of $\Delta G^{\neq}_{exp} = 13.2$–$12.9$ kcal mol^{-1} as calculated from the experimental rate constants for H_2O_2 decomposition by complexes **1**, **2** and their derivatives ($k_{exp} = (1.3$–$2.3) \times 10^3$ M^{-1} s^{-1} at 20 °C).[30] The strikingly close correspondence of the experimental and computed activation free energies thus further supports a homolytic route for the cleavage of the first associated molecule of H_2O_2 in the catalytic process.

The spin densities in ^{2}**8a**, ^{2}**8b**, and ^{4}**8** (Figure 4) provide information on the electron redistribution during the bond-breaking process. The unpaired spin density in the parent complexes ^{2}**7a,b** and ^{4}**7** is largely concentrated on iron ($\rho_{Fe} =$ 0.98 and 2.64, respectively) with negligible contribution from the ligands. On O–O bond elongation, in each case a spin density of about $\rho_O = 0.5$ evolves on the terminal OH group of the coordinated H_2O_2. This indicates the onset of homolytic bond cleavage with release of an HO• radical and iron bonding of an hydroxyl anion. In ^{2}**8a**, the positive spin density on the iron center is increased to $\rho_{Fe} = 1.31$, but the increase is largely compensated by a negative spin density on the leaving OH group. Only a minor fraction of spin is transferred to the macrocyclic ligand ($\rho_L = 0.19$). Contrarily, in ^{2}**8b** the positive spin density of $\rho_{Fe} = 0.99$ on the iron center is retained, because the positive spin density of $\rho_O =$ 0.5 on the terminal OH group is accompanied by development of an equal spin density of opposite sign on the π system of the macrocyclic ligand. This spin distribution is indicative of one-electron oxidation of the ligand to its radical cation. The oxygen atoms of both iron-bound OH groups in ^{2}**8a,b** carry only negligible spin density, which shows their hydroxide-anion character, whereas in ^{4}**8** some spin density ($\rho_O = 0.28$) is found on the proximal OH ligand.

When the O–O distance in TS ^{2}**8a** was elongated to 2.1 Å, subsequent geometry optimization did not lead to a complete expulsion of HO• radical and formation of the triplet-state dihydroxy complex ^{3}**9**, but rather provided ground-state product ^{2}**10** (Figure 5), in which the released HO• radical remains closely associated with dihydroxy complex ^{3}**9**. Formation of ^{2}**10** is downhill by −3.1 kcal mol^{-1} with respect to the parent H_2O_2 complex ^{2}**7a**. The ^{3}**9**–HO• interaction (^{3}**9** + HO• → ^{2}**10**), which energetically amounts to −14.1 kcal mol^{-1} (Table 1, Figure 2), is clearly reflected by the structural parameters and the corresponding spin-density distribution (Figure 5), that is, ^{2}**10** is not only stabilized by a rather strong Fe(HO)···HO• hydrogen bond ($r = 1.703$ Å) but also

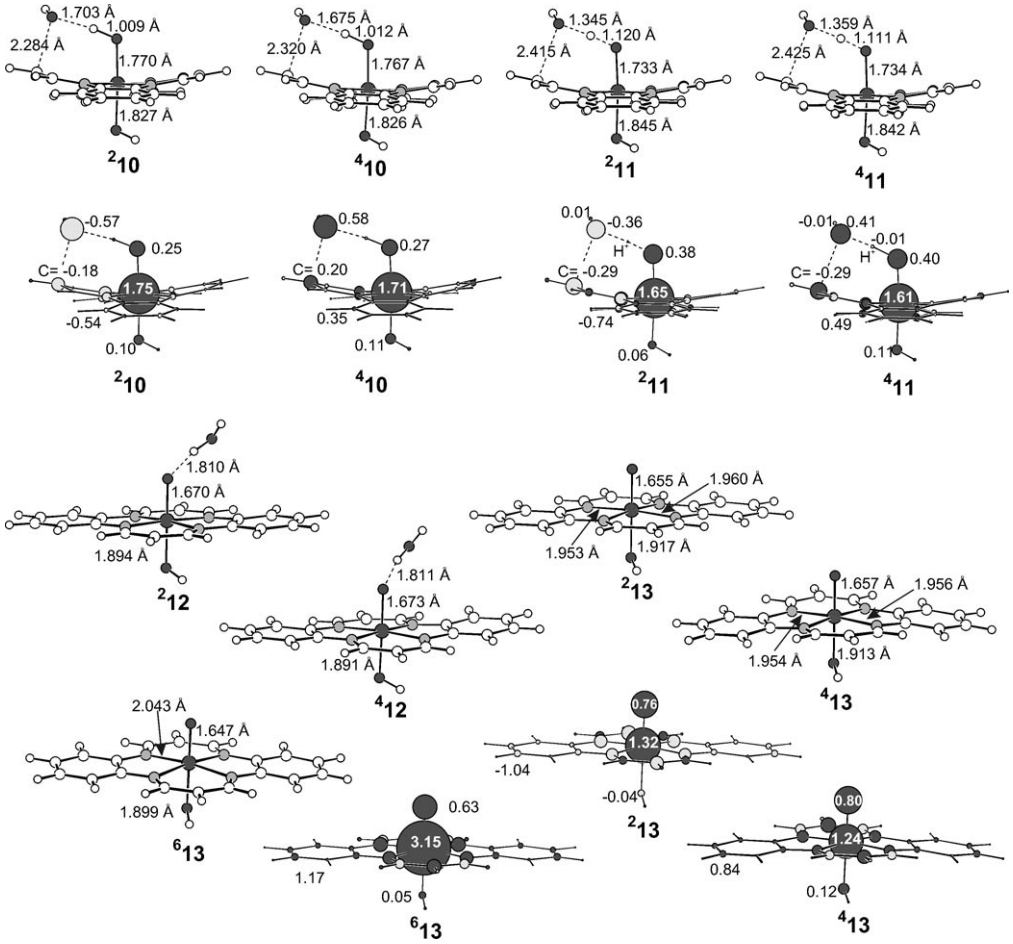

Figure 5. Calculated structures and spin densities of complexes **10**–**13**.

characterized by evolution of significant negative spin density ($\rho_L = -0.54$) on the macrocyclic ligand. Simultaneously, the spin density on iron is increased to $\rho_{Fe} = 1.75$. Thus, the spin density pattern in ^{2}**10** indicates the onset of a one-electron oxidation of the macrocycle by the HO$^\bullet$ radical. This is supported by the transition structure ^{2}**11**, which was found starting from ^{2}**10**. In ^{2}**11**, the spin density on the macrocyclic ligand is increased to $\rho_L = -0.74$, concomitantly with a decrease of the spin density on the associated hydroxyl radical ($\rho_O = -0.36$). The distance of the HO$^\bullet$ oxygen atom to the hydrogen atom of the distal iron-bound hydroxyl group is shortened to 1.345 Å and the H–OFe bond length elongated to 1.120 Å . The shortest distance of the oxygen atom of the hydroxyl radical to the macrocycle is found for the *meso*-carbon atom of the isopropylidene group (2.415 Å). These data and the displacement vector of the imaginary eigenfrequency ($\tilde{\nu}_i = 957.5\,i\,cm^{-1}$) along the O···H···O direction reveal that TS ^{2}**11** corresponds to proton transfer from the iron-bound OH group to the hydroxyl radical with simultaneous transfer of an electron from the [N_4] macrocycle to the HO$^\bullet$ radical. Hence, TS ^{2}**11** can be regarded as an example of proton-coupled electron transfer (PCET) via a seven-membered transition state. However, the associated barrier is negligibly small; in fact, the ZPVE-corrected energy of ^{2}**11** is even lower (by -1.1 kcal mol^{-1}) than that of the preceding complex ^{2}**10**. This artifact is caused by the difference in the computed ZPVEs and is a consequence of the harmonic approximation and the "loss" of the imaginary frequency mode corresponding to the reaction coordinate in the TS. Without ZPVE correction ^{2}**11** is found to be 1.4 kcal mol^{-1} higher in energy than ^{2}**10**. The PCET-type hydrogen-transfer process via TS ^{2}**11** finally yields ferryl oxo (Fe^{IV}=O) species ^{2}**12**, to which the produced water molecule remains hydrogen-bonded.

Interestingly, the same aqua ferryl oxo complex ^{2}**12** was also reached from transition state ^{2}**8b**, in which the [N_4] ligand is already partially oxidized. After elongation of the O–O bond to 2.1 Å, subsequent optimization resulted in barrierless rotation of the iron-bound OH group in the direction of the oxygen atom of the leaving OH group, concomitantly with barrierless hydrogen-atom transfer to the evolving hydroxyl radical. The failure to locate an HO$^\bullet$ complex similar to ^{2}**10** may be related to weaker hydrogen-bonding interaction of the liberated HO$^\bullet$ group with the more positively charged macrocycle. Alternative release of free HO$^\bullet$ radical and formation of the singlet-state ($S = 0$) dihydroxy complex ^{1}**9** (Figure 4) was computed to be uphill by 4.7 kcal mol^{-1}.

Formation of ^{2}**12** from ^{2}**7a,b** is energetically downhill by -19.4 kcal mol^{-1} (-23.6 kcal mol^{-1} from the starting complex ^{4}**2**+H_2O_2), of which -9.8 kcal mol^{-1} is provided by the hydrogen bond between the produced water molecule and ferryl oxo complex ^{2}**13**. This magnitude of hydrogen bond strength is characteristic for sp^2-O···HO hydrogen bonds computed at the present DFT level[57]. The spin-density distributions in complex ^{2}**12** and related free ferryl oxo species ^{2}**13** clearly show that the Fe^{IV}=O center is coordinated by a π-type radical cation of the macrocycle. The system comprises three unpaired electrons, two of which reside in π^*_{FeO} orbitals on the distal Fe=O group and one in an b_{1u} π orbital on the macrocyclic ligand (see Scheme S1 in the Supporting Information). The doublet spin multiplicity of the starting complexes ^{2}**7** is preserved in ^{2}**12**/^{2}**13** due to antiferromagnetic coupling of the unpaired electrons, which induces negative spin density on the macrocycle. Species ^{2}**13** is electronically equivalent to Compound I of the catalase or cytochrome families of heme enzymes. As was pointed out by Shaik et al., the spin distribution in the ferryl oxo species of iron porphyrins can be considered to be the same as in triplet oxygen.[20,21,58] The singly occupied b_{1u} π orbital of the macrocyclic ligand resembles the singly occupied a_{2u} orbital of the porphyrin ligand in Compound I.[20,36]

On the quartet-state surface, the O–O bond-breaking process via transition state ^{4}**8** turned out to be structurally and energetically very similar to the doublet pathway starting from ^{2}**7a**. After O–O bond elongation, complex ^{4}**10**, intermediate between HO$^\bullet$ radical and the same triplet-state ($S = 1$) dihydroxy complex ^{3}**9** as formed from ^{2}**8a**, was located. Like for ^{2}**10**, further reaction proceeds by proton-coupled electron transfer via transition structure ^{4}**11** with a negligible barrier (1.0 kcal mol^{-1} at the SCF level, but -1.4 kcal mol^{-1} in terms of ZPVE-corrected energy). Differently to ^{2}**11**, less spin density is transferred to the macrocycle ($\rho_L = 0.49$). The PCET product, aqua complex ^{4}**12**, is energetically almost identical to its doublet-state counterpart ^{2}**12**. Its formation is exoergic by -23.5 kcal mol^{-1} from the initial complex ^{4}**2**+H_2O_2 or -19.0 kcal mol^{-1} from the hydrogen peroxide complex ^{4}**7**. The spin-density distribution in the triradicaloid quartet-state complex ^{4}**12** and the related free ferryl oxo species ^{4}**13** is similar to that computed for ^{2}**12** and ^{2}**13**, respectively, but now reflects ferromagnetic coupling between the two unpaired electrons on the Fe^{IV}=O group and the unpaired spin on the ligand (see Scheme S2 in the Supporting Information). The coupling between the π^*_{FeO} orbitals and the ligand π orbital, however, is very small. On the SCF level, ^{4}**12** and ^{4}**13** were computed to be stabilized by -0.10 and -0.12 kcal mol^{-1}, respectively, over doublet species ^{2}**12**, ^{2}**13**, whereas after ZPVE correction a minuscule preference for ^{2}**12** and ^{2}**13** (-0.06 and -0.02 kcal mol^{-1} respectively) was predicted. Hence, the doublet and quartet states of species ^{2}**13** and ^{4}**13** are essentially degenerate. A similar doublet–quartet spin degeneracy has also been proposed for ferryl oxo porphyrin species.[20,21] The computed structure of the Fe^{IV}=O moiety of **13** is comparable to that published recently for heme and non-heme Fe^{IV}=O species by Decker and Solomon,[59] who showed that the geometry of this subunit does not depend on the nature of the ligand, whether heme or non-heme in character. In accord, our computed Fe–O bond lengths (^{2}**13**: 1.655, ^{4}**13**: 1.657, ^{6}**13**: 1.647 Å) match the experimental data of 1.62–1.7 Å for horseradish peroxidase Compound I excellently.[12] In any case, a sextet-state ($S = 5/2$) pathway for the first stage of catalase-like hydrogen peroxide decomposition is improbable, as deduced from the failure to locate a corresponding transition state

(^{6}**8**; see above) and the higher energies of structures ^{5}**9**, ^{6}**12**, and ^{6}**13**, which (hypothetically) would be produced via such a route.

The general picture outlined above did not change when aqueous solvation was considered. In correspondence with the gas-phase data, Compound I analogues ^{2}**13** and ^{4}**13** were found to differ by only 0.2 kcal mol^{-1}, but ^{6}**13** was calculated to be about 17 kcal mol^{-1} higher in energy (Table 1, see Figure S3 in the Supporting Information). The ferryl oxo species **13** are predicted to be more stabilized in aqueous solvation, by about 5–6 kcal mol^{-1}, than in the gas phase, that is, formation of ^{2,4}**13** plus water from the reference level ^{4}**2** + H_2O_2 is downhill by 19–20 kcal mol^{-1}.

The foregoing results strongly suggest that the first step of hydrogen peroxide cleavage by our catalysts is in fact homolytic in nature. The homolytic O–O bond dissociation enthalpy (BDE) of gaseous H_2O_2 is 51.1 ± 0.1 kcal mol^{-1}.[60] The calculated values compare favorably with the experimental data (see Table S5 in the Supporting Information). Since the recombination of two HO$^{\bullet}$ radicals is essentially barrierless, the BDE should be very close to the activation energy for O–O homolysis. Comparison with the 10.6/12.0 and 18.2 kcal mol^{-1} activation energy required for O–O cleavage in complexes ^{2}**7a**,**b** and ^{4}**7**, respectively, thus reveals a strong catalytic effect of iron.[24] As indicated by the spin-density distribution in transition structures ^{2}**8a**,**b** and ^{4}**8**, this can be related to electron transfer from the iron center and, further, from the ligand π system to the iron-bound oxygen atom, that is, H_2O_2 is essentially cleaved to hydroxyl radical and hydroxide anion. The origin of similarly low O–O bond dissociation energies in iron(III) porphyrin hydroperoxide complexes has recently been discussed more thoroughly by Bach and Dmitrenko.[52]

Reaction of the ferryl oxo species with hydrogen peroxide: Since the foregoing calculations indicate that our catalase mimic is likely to produce an intermediate ferryl oxo species similar to Compound I of native catalase, which may exist in two almost degenerate spin states (^{2}**13**/^{4}**13**), the computational modeling of its reaction with the second hydrogen peroxide molecule was carried out for both spin states. Due to the significantly higher energy of intermediate ^{6}**13** (see above), the sextet-state route was not further considered. As ^{2}**13** and ^{4}**13** solely differ in the relative spin of the unpaired electron in the π-radical cation, thermal spin-crossover equilibrium between the two species is conceivable. Thus, due to the little energy required for spin flip, it was expected that both reaction paths would be energetically equivalent. This indeed turned out to be the case, as outlined in the following.

As starting structures for the reaction of H_2O_2 with the ferryl oxo intermediate in its two spin states (^{2,4}**13**), two possible arrangements of hydrogen peroxide relative to the oxy ferryl group were considered: linear ("end-on", ^{2,4}**14a**), in which H_2O_2 is singly hydrogen bonded to the ferryl oxygen atom, and a cyclic ("side-on", ^{2,4}**14b**) in which hydrogen peroxide adopts a synperiplanar conformation and forms two cooperative hydrogen bonds to the Fe^{IV}=O group (Figure 6). Energies are given relative to ^{2}**13** + H_2O_2 (Table 3, Figure 7; see Figures S5, S6 in the Supporting Information for enthalpy and free-energy schemes). As is evident from the energy data, the doublet and quartet pathways for oxygen production are in fact equivalent; the energies of the two states differ by not more than 0.2 kcal mol^{-1}. Likewise, the geometries of related structures are very similar. Therefore, in Figures 6, 8–10 only the doublet-state structures are reproduced; the quartet-state structures are given in Schemes S3, S4 in the Supporting Information. In the following, the numerical values for the doublet and quartet states are separated by a slash.

In both spin states, the cyclic arrangements ^{2,4}**14b** are slightly, that is, 0.9 and 1.0 kcal mol^{-1}, higher in energy than the linear structures ^{2,4}**14a**. In ^{2,4}**14a** an almost linear hydrogen bond between the ferryl oxo group and hydrogen peroxide (∢(OHO) = 174/169°) with an FeO–H distance of 1.723/1.724 Å is found. This hydrogen bonding results in a stabilization of 11.6 kcal mol^{-1} with respect to the isolated reactants (Figure 7). An OH···π interaction of the peroxide terminal OH group with the *meso*-carbon atom of the macrocyclic ligand (OH–C 2.533/2.538 Å) is likely to contribute to

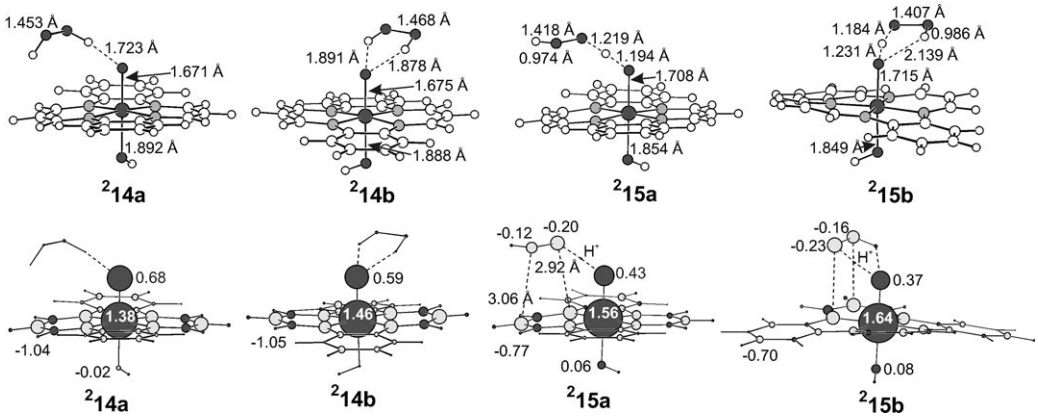

Figure 6. Calculated structures and spin densities of complexes **14** and **15**.

Table 3. Relative (U)B3LYP/6-31G* energies [kcal mol^{-1}] for reaction of Fe^{IV}=O species **13** with H_2O_2.[a]

Compound	ΔE^0	ΔE^0+ZPVE	ΔH^{298K}	ΔG^{298K}
^{2}**2**+H_2O+O_2	−30.09	−31.8	−31.0	−40.8
^{4}**2**+H_2O+O_2	−32.24	−35.0	−33.8	−44.4
^{2}**6**+O_2	−40.28	−39.8	−39.6	−39.2
^{4}**6**+O_2	−37.26	−38.8	−37.5	−40.6
^{3}**9**+$^{\cdot}$OOH	−10.97	−11.3	−11.4	−11.5
^{2}**13**+H_2O_2	**0.0**	**0.0**	**0.0**	**0.0**
^{4}**13**+H_2O_2	−0.12	0.0	−0.1	−0.3
^{2}**14a**	−13.16	−11.6	−11.7	−1.0
^{4}**14a**	−13.27	−11.6	−11.8	−1.6
^{2}**14b**	−12.13	−10.7	−10.7	−0.5
^{4}**14b**	−12.24	−10.6	−10.7	−0.7
^{2}**15a**	−5.36	−7.1	−7.6	4.2
^{4}**15a**	−5.48	−7.3	−7.7	3.7
^{2}**15b**	−5.83	−7.0	−7.8	4.9
^{4}**15b**	−6.01	−7.1	−7.9	4.5
^{2}**16a**	−19.94	−18.5	−18.8	−7.8
^{4}**16a**	−19.97	−18.6	−18.9	−8.3
^{2}**17a**	−27.56	−27.3	−27.5	−16.6
^{4}**17a**	−27.75	−27.4	−27.8	−16.9
^{2}**17b**	−26.63	−25.3	−25.5	−14.9
^{4}**17b**	−26.67	−25.4	−25.6	−15.4
^{2}**18**	−27.50	−28.5	−29.2	−17.3
^{4}**18**	−27.68	−28.7	−29.4	−17.7
^{2}**19**	−42.97	−41.8	−41.5	−32.4
^{4}**19**	−43.00	−41.9	−41.5	−32.8

[a] Energies relative to ^{2}**13**+H_2O_2.

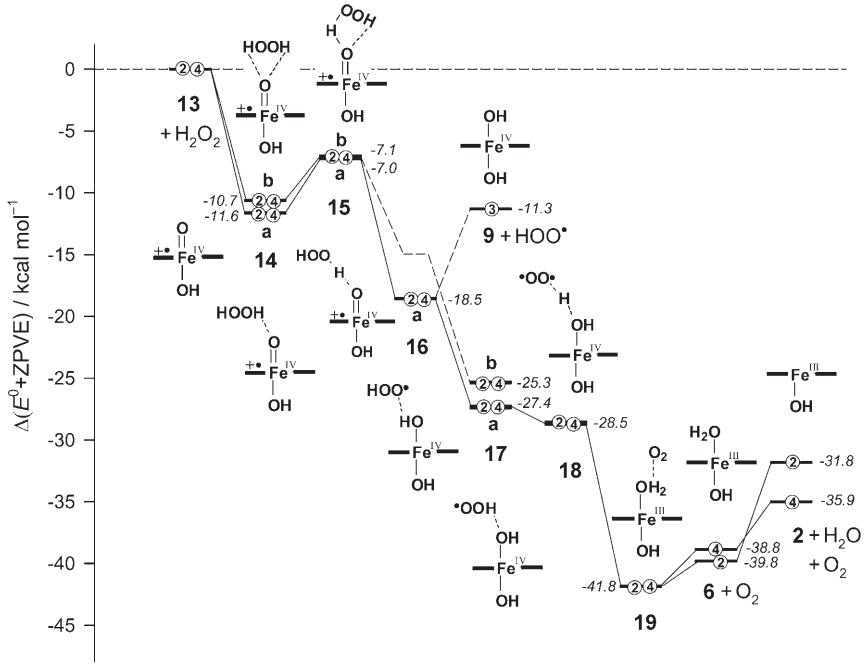

Figure 7. Energy (0 K) scheme for reaction of Fe^{IV} oxo species **13** with hydrogen peroxide. Encircled numbers denote the spin multiplicities; the macrocyclic ligand is symbolized by solid horizontal bars.

the hydrogen-bond strength, as indicated by a reduced O–H vibrational frequency ($\nu(OH)_{terminal}$ = 3675/3676 cm^{-1}) compared to free H_2O_2 ($\nu(OH)_{as}$ = 3708 cm^{-1}). The hydrogen-bond lengths to the ferryl oxygen atom in the cyclic structures ^{2,4}**14b** are rather short (1.890/1.887 and 1.878/1.880 Å, respectively). Thus, it appears that the additional hydrogen bond in the cyclic H_2O_2 arrangement compensates for the energy required for rotation of the gauche (111.8°[61,62]) ground-state (gas-phase) conformation of H_2O_2 into its syn-periplanar conformation (*cis* barrier), which for gaseous H_2O_2 is in fact a rotational transition state with $\Delta E^{\neq}$ = 7.1–7.4 kcal mol^{-1} (Table 2, footnote [e]).[61–64]

Association of H_2O_2 with the parent ^{2,4}**13** results in some increase of the unpaired spin density on iron for both arrangements and spin states ($\Delta\rho_{Fe}$ = 0.06–0.16, Figure 6), but the spin on the macrocycle remains almost unchanged. No unpaired spin density is transferred to the associated hydrogen peroxide.

Starting from elongated O–H bonds in ^{2,4}**14a**, transition structures ^{2,4}**15a** for hydrogen-atom transfer to the ferryl oxo group were located in which the hydrogen atom resides almost symmetrically between the two oxygen atoms (Figure 6), at distances of 1.219 and 1.194 Å. The activation barrier for this process is rather low, 4.5 kcal mol^{-1} (Figure 7), which in fact would be expected for the known high ("OH-radical-like") reactivity of Compound I-type species.[17,21] Complete transfer of the hydrogen atom is exoergic by −18.5 kcal mol^{-1} and leads to complexes ^{2,4}**16a** in which the produced hydroperoxyl radical remains hydrogen-bonded to the dihydroxy-Fe^{IV} complex ^{3}**9** (Figure 8). The stabilization energies of −7.2/−7.3 kcal mol^{-1} of the HOO$^{\cdot}$···HOFe hydrogen bonds (2.027/2.025 Å) in ^{2,4}**16a** (vs. ^{3}**9**+HOO$^{\cdot}$) seems to involve a contribution from OH···π contacts (2.044/2.041 Å) to a *meso*-C atom of the macrocycle, similar to the bonding of H_2O_2 in the starting complexes ^{2,4}**14a**. The two iron-bound hydroxyl groups in ^{2,4}**16a** each form a single hydrogen bond to the two adjacent nitrogen atoms of a phenylene moiety, and thus they are fixed in an 128-degree dihedral arrangement. The doublet and quartet structures simply differ by the sign of the unpaired spin density on the evolving hydroperoxide radical/oxygen molecule. During the hydrogen-transfer process the total unpaired spin density on the HOFe^{IV}=O moiety changes only marginally in going from ^{2,4}**14a** (ρ_{HOFeO} = 2.04/2.15) via transition structures ^{2,4}**15a** (ρ_{HOFeO} = 2.07/2.12) to complexes ^{2,4}**16a** (ρ_{HOFeO} = 2.10/2.10), but the relative spin distribution within this group is shifted in favor of the Fe–OH_{prox} moiety. On the way to TS ^{2}**15a**, some negative spin density (ρ_{OO} = −0.33) evolves on the oxygen atoms of the hydrogen perox-

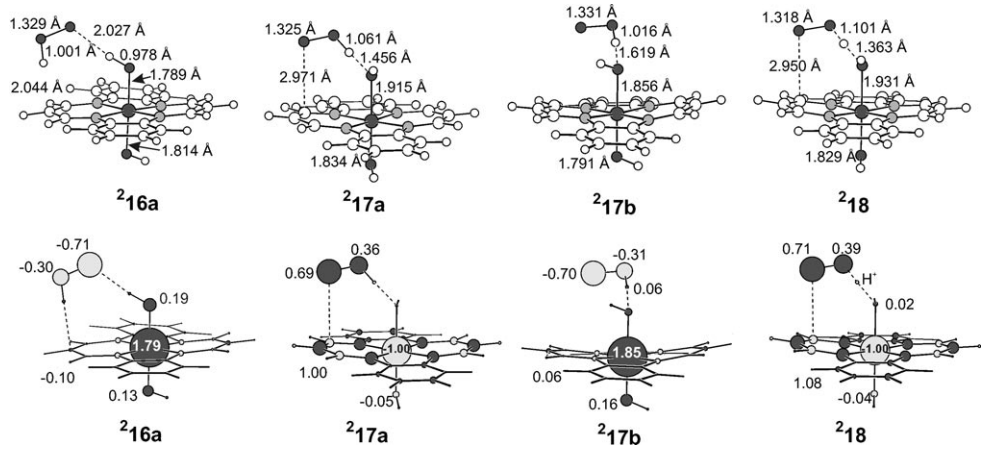

Figure 8. Calculated structures and spin densities of complexes **16**–**18**.

ide unit; in the quartet structure ^{4}**15a** the positive hydroperoxide spin density is of similar size ($\rho_{OO}=0.37$). These increases are accompanied by a similar reduction of the spin density on the macrocycle ($\Delta\rho_L=0.27/0.32$). In products ^{2,4}**16a** (nearly) two unpaired electrons reside on the iron center ($\rho_{Fe}=1.78/1.79$) and the hydroperoxyl radical carries one unpaired electron ($\rho_{HOO}=-1.01/1.02$), but only little spin density ($\rho_L=-0.12/-0.12$) is found on the macrocycle. Thus, the development of the spin-density distribution again indicates that a PCET process take places, that is, reduction of the π-radical cation ligand via electron transfer from hydrogen peroxide simultaneously with transfer of a proton to the ferryl oxo group.

To complete the formation of molecular oxygen, the associated hydroperoxyl radical in ^{2,4}**16a** must transfer a hydrogen atom to the distal OH group. In fact, on further optimization after elongation of the hydrogen bond in ^{2,4}**16a** by 0.2 Å, the HOO$^\bullet$ group underwent a barrierless "somersault"[52] rearrangement to the hydrogen-bonded structures ^{2,4}**17a**, in which the hydroperoxyl radical now acts as the hydrogen donor to the distal OH group. Noteworthily, in structures ^{2,4}**17a** the hydroperoxyl radical is 8.7/8.8 kcal mol^{-1} more strongly bound than in structures ^{2,4}**16a** (Figure 7). The strong hydrogen bond (−15.8 kcal mol^{-1} vs. ^{3}**9** + HOO$^\bullet$) is reflected by a short $^\bullet$OOH···OFe distance of 1.456 Å, in line with a high negative partial charge ($q_O=-0.86$) on the distal oxygen atom. The axial OH ligands in ^{2,4}**17a** are now found in a synperiplanar arrangement along the *x* axis, and both form a bifurcated hydrogen bond to the same adjacent nitrogen atoms of the macrocycle.

The spin-density distribution in ^{2,4}**17a** shows rather surprising features (Figure 8). Different to complexes ^{2,4}**16a**, in which two unpaired electrons are located on iron, in ^{2,4}**17a** only one unpaired electron is found on iron ($\rho_{Fe}=-1.00/+1.00$), but the macrocyclic ligand is predicted to be reoxidized to its π-radical cation. In addition, in ^{2}**17a** the relative signs of the spin densities are reversed compared to the foregoing complexes, and now negative spin density is found on iron, and positive spin on the macrocycle and on the hydroperoxyl fragment. (Deeper insight into this dramatic change in the electronic configuration on the way from the local minimum ^{2}**16a** to the local minimum ^{2}**17a** could only be achieved by use of configuration interaction methods, which is beyond the scope of this paper.)

Decomposition of H_2O_2 via cyclic complexes ^{2,4}**14b** proceeded similarly, with the exception that no stable hydroperoxyl complexes like ^{2,4}**16a** could be located. The barriers (3.7/3.5 kcal mol^{-1}) for transfer of the first hydrogen atom are smaller (0.8/0.9 kcal mol^{-1}) by just the difference in the ground-state energies of the starting complexes, and thus transition structures ^{2,4}**14b** are on the same energetic level as ^{2,4}**14a**. On following the reaction path further, hydrogen transfer and rotation of the hydroperoxyl residue occurred continuously and led directly to the hydroperoxyl complexes ^{2,4}**17b**. These complexes are 2.1/2.2 kcal mol^{-1} less stabilized than the "**a**" structures, most likely due to the different orientation of the axial hydroxyl groups giving rise to weaker hydrogen bonding in the "**b**" conformations. Due to the otherwise identical characteristics to the "**a**" path, further reaction of these complexes was not pursued.

From hydroperoxyl complexes ^{2,4}**17a**, the bridging hydrogen atom is transferred essentially without barrier to the distal OH group because the corresponding transition structures ^{2,4}**18** were computed to be just 0.1 kcal mol^{-1} above ^{2,4}**17a** on the SCF level, and even lower in energy, by about 1.3 kcal mol^{-1}, after ZPVE correction (see above). Note that the spin distribution of ^{2}**18** is already preformed in ^{2}**17a**, which helps to understand the low barrier in this case. In TSs ^{2,4}**18**, the spin density on the hydroperoxyl group is slightly increased with respect to ^{2,4}**17a**, similar to what was found for TSs ^{2,4}**15a**. This again implies that the reaction proceeds by a PCET mechanism. In fact, in the final reaction products ^{2,4}**19** the macrocycle is completely re-reduced with one unpaired electron remaining on the iron center (Figure 9). Oxygen remains weakly (−2.0/−3.0 kcal mol^{-1}) associated with the water ligand (Figure 7). Noteworthily, molecular oxygen is directly produced in its triplet ground state rather than in the reactive singlet excited state, which

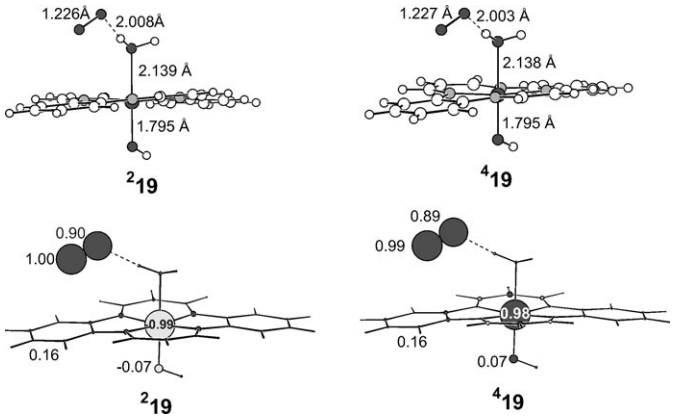

Figure 9. Calculated structures and spin densities of complexes **19**.

is harmful to living organisms. Although such a mechanism of oxygen production as depicted here cannot be expected to be that operating in native catalase (in which a distal histidine residue is assumed to play a crucial role as a proton shuttle[8–10]), it is in line with the observation that both atoms of the released oxygen molecule stem from the same H_2O_2 molecule.[56]

The ^{2,4}**17a**$\rightarrow$^{2,4}**19** hydrogen-transfer step is energetically downhill by -14.5 kcal mol^{-1}, and this renders the overall reaction from ^{2}**13**$+H_2O_2$ highly exoergic (-41.8 kcal mol^{-1}). Dissociation of oxygen and water from ^{2,4}**19** requires 2.0/3.0$+$7.9/2.9$=$9.0/5.9 kcal mol^{-1} to regenerate the hexa- and pentacoordinate starting complexes ^{2,4}**6** and ^{2,4}**2**, respectively, that is, the "resting state" of our catalase mimic is reestablished.

At this point the total energy balance for reaction of ^{2}**2** and ^{4}**2** with two molecules of hydrogen peroxide can be derived. In the first stage (Figure 2)—formation of the Compound I-analogous ferryl oxo species ^{2}**13**, ^{4}**13** and water—net energies of -17.1 and -13.9 kcal mol^{-1} are released on the doublet and quartet paths, respectively. The second stage (Figure 7)—formation of water, molecular oxygen and regeneration of ^{2}**2** or ^{4}**2**—provides -31.8 and -35.9 kcal mol^{-1}, respectively. The sum of both equals the reaction energy for Equation (1) of $\Delta_1E^0+\mathrm{ZPVE})=-48.8$ kcal mol^{-1}. The corresponding enthalpy value is slightly lower, $\Delta_1H^{298\,\mathrm{K}}=-47.3$ kcal mol^{-1}. With regard to the known tendency of the applied DFT procedure to underestimate heats of formation/bond dissociation energies, these values compare very well with the experimental reaction enthalpy of Δ_1H-(exp)$^{298\,\mathrm{K}}=-50.6$ kcal mol^{-1}[60] (see Table S5 in the Supporting Information). For comparison purposes, values for hydrogen abstraction from hydrogen peroxide by hydroxyl radical and for the dismutation of two hydroperoxy radicals to hydrogen peroxide and oxygen are also listed in Table S5 in the Supporting Information, and they again show good agreement with the corresponding experimental values.[60]

Catalyst deactivation: The turnover numbers for H_2O_2 decomposition by complex **1** and its analogues have been determined to be in the range of 40–80 mol H_2O_2 per mole catalyst, that is, after these numbers of catalytic cycles the catalysts become deactivated.[29,30] In view of the high reactivity of the above-discussed intermediates, deactivation may reasonably be related to self-destruction of the complexes by oxidative attack on the [N_4] macrocyclic ligand, similar to the known oxidative degradation of iron porphyrins.[54,65] Fractional release of free HO$^\bullet$ radicals (to give ^{1,3}**9**) may be a viable side reaction, although in reality HO$^\bullet$ should be effectively trapped by the large excess of H_2O_2. In fact, in the presence of excess DMSO, products have been detected which are very characteristic for the intermediacy of free HO$^\bullet$ radicals.[29,30] For cytochrome P450-mediated oxidations it has recently been proposed that a hydrogen-bonded ferryl oxo$\cdots$HO$^\bullet$ complex may be a viable active oxidant, which can be expected to react like a freely diffusing HO$^\bullet$ radical.[52,53] Thus, deactivation might more reasonably be assumed to be due to intramolecular attack of HO$^\bullet$ radicals produced in the **7**$\rightarrow$**12** process and locked in the coordination sphere of iron, that is, simply formed from complexes **10** by rotational reorientation. In line with this hypothesis, a quartet-state structure (^{4}**20**) was found in which the released HO$^\bullet$ radical forms a hydrogen bond to dihydroxy complex ^{3}**9** (Figure 10). Complex ^{4}**20** is only 3.2 kcal mol^{-1} less stable

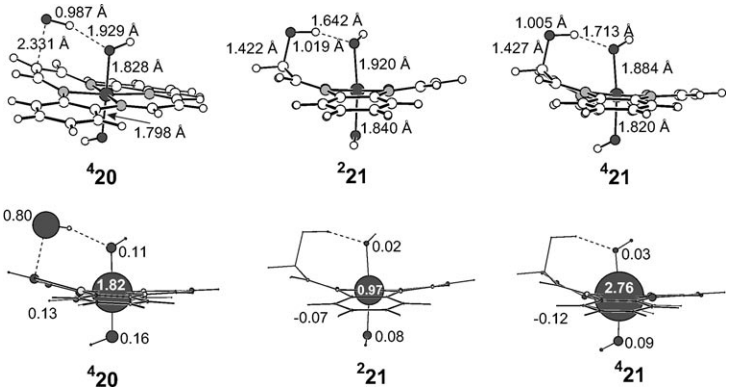

Figure 10. Calculated structures and spin densities of complexes **20** and **21**.

than complex ^{4}**10**. From ^{4}**20**, the HO$^\bullet$ radical then undergoes facile addition to the *meso*-carbon atom of the macrocycle to give hydroxylated product ^{4}**21**. A corresponding doublet-state HO$^\bullet$ complex ^{2}**20** could not be found. Rather, after minor rearrangement of the HO$^\bullet$ group of ^{2}**10**, subsequent optimization directly led to barrierless addition of HO$^\bullet$ to the *meso* position of the macrocycle to give hydroxyl adduct ^{2}**21.** Thermochemically, this addition reaction is favorable; it is exoergic by -30.4 kcal mol^{-1} on the quartet surface (from ^{4}**2**$+H_2O_2$), and by as much as -49.5 kcal mol^{-1} on the doublet surface (from ^{2}**2**$+H_2O_2$). This putative reaction again would model the chemistry of native heme oxidases, for which a similar mode of porphyrin-ligand oxidation has recently been proposed.[24,53,54]

Conclusion

The computational data presented here demonstrate that hydrogen peroxide decomposition by the 14-membered macrocyclic tetraaza Fe^{III} complex **2** and its analogues largely mimics the mechanism that has been established for H_2O_2 disproportionation by native catalase. The data predict that the reaction may proceed on the doublet-spin ($S=^1/_2$) and quartet-spin ($S=^3/_2$) surfaces. In a rate-limiting first step, a ferryl oxo ligand radical cation intermediate ($L^{\bullet+}Fe^{IV}=O$) is formed via homolytic O–O bond cleavage of a coordinated H_2O_2 molecule, followed by hydrogen transfer to the thus-produced hydroxyl radical by means of a PCET mechanism, with an exothermicity of -14 to -17 kcal mol^{-1}. Remarkably, the transition state for O–O homolysis is the only structure found for which a significant energetic preference for a certain spin state is predicted: the doublet-state path is kinetically favored over the quartet-state path by 6–8 kcal mol^{-1}. The ferryl oxo intermediate, which strikingly resembles Compound I of native catalase, is predicted to exist in nearly degenerate doublet and quartet spin states.

In a second, low-barrier and highly exoergic ($\Delta E=-32$ to -36 kcal mol^{-1}) process, reaction of this Compound I analogue with a second molecule of H_2O_2 again proceeds homolytically to produce molecular oxygen directly in its triplet ground state with regeneration of the resting state of the Fe^{III} complex. Structurally and energetically, no significant difference between the doublet- and quartet-state paths was found.

The computations also suggest a viable mode for deactivation of the catalyst by addition of the released $HO^{\bullet}$ radical to the macrocyclic ligand of its precursor complex.

Acknowledgements

The generous allocation of computer resources by the Hochschulrechenzentrum der Universität Duisburg-Essen is gratefully acknowledged. This work was supported by the Deutsche Forschungsgemeinschaft (SFB 452). We are indebted to two anonymous referees for valuable suggestions.

[1] U. Rauen, U. Kerkweg, D. Weisheit, F. Petrat, R. Sustmann, H. de Groot, *Free Radical Biol. Med.* **2003**, *35*, 1664–1678.
[2] U. Rauen, T. Li, R. Sustmann, H. de Groot, *Free Radical Biol. Med.* **2004**, *37*, 1369–1383.
[3] U. Rauen, F. Petrat, T. Li, H. de Groot, *FASEB J.* **2000**, *14*, 1953–1964.
[4] U. Rauen, F. Petrat, R. Sustmann, H. de Groot, *J. Hepatol.* **2004**, *40*, 605–613.
[5] B. Halliwell, J. M. C. Gutteridge, *Methods Enzymol.* **1990**, *186*, 1–85.
[6] S. P. Young, P. Aisen in *The Liver: Biology and Pathology* (Eds.: I. M. Arias, J. L. Boyler, N. Fausto, W. B. Jakoby, D. A. Schachter,-D. A. Shafritz), Raven Press, New York, **1994**, pp. 597–617.
[7] F. Petrat, H. de Groot, R. Sustmann, U. Rauen, *Biol. Chem.* **2002**, *383*, 489–502.
[8] G. R. Schonbaum, B. Chance in *The Enzymes, Vol. 13* (Ed. P. D. Boyer), Academic Press, New York, **1976**, pp. 363–408.
[9] M. Zamocky, F. Koller, *Prog. Biophys. Mol. Biol.* **1999**, *72*, 19–66.
[10] P. Nicholls, I. Fita, P. C. Loewen, *Adv. Inorg. Chem.* **2001**, *51*, 51–106.
[11] M. J. Benecky, J. E. Frew, N. Scowen, P. Jones, B. M. Hoffman, *Biochemistry* **1993**, *32*, 11929–11933.
[12] G. I. Berglund, G. H. Carlsson, A. T. Smith, H. Szöke, A. Henriksen, J. Hadju, *Nature* **2002**, *417*, 463–468.
[13] M. Newcomb, R. Zhang, R. E. P. Chandrasena, J. A. Halgrimson, J. H. Horner, T. M. Makris, S. G. Sligar, *J. Am. Chem. Soc.* **2006**, *128*, 4580–4581.
[14] E. Derat, S. Shaik, *J. Phys. Chem. B* **2006**, *110*, 10526–10533.
[15] W. Nam, Y. O. Ryu, W. J. Song, *J. Biol. Inorg. Chem.* **2004**, *9*, 654–660.
[16] S. Shaik, S. P. de Visser, D. Kumar, *J. Biol. Inorg. Chem.* **2004**, *9*, 661–668.
[17] I. G. Denisov, T. M. Makris, S. G. Sligar, I. Schlichting, *Chem. Rev.* **2005**, *105*, 2253–2278.
[18] M. J. Park, J. Lee, Y. Suh, J. Kim, W. Nam, *J. Am. Chem. Soc.* **2006**, *128*, 2630–2634.
[19] H. Hirao, D. Kumar, W. Thiel, S. Shaik, *J. Am. Chem. Soc.* **2005**, *127*, 13007–13018.
[20] S. Shaik, D. Kumar, S. P. de Visser, A. Altun, W. Thiel, *Chem. Rev.* **2005**, *105*, 2279–2328.
[21] B. Meunier, S. P. de Visser, S. Shaik, *Chem. Rev.* **2004**, *104*, 3947–3980.
[22] P. Rydberg, E. Sigfridson, U. Ryde, *J. Biol. Inorg. Chem.* **2004**, *9*, 203–223.
[23] M. T. Green, *J. Am. Chem. Soc.* **2001**, *123*, 9218–9219.
[24] E. Derat, D. Kumar, H. Hirao, S. Shaik, *J. Am. Chem. Soc.* **2006**, *128*, 483–484.
[25] S. V. Kryatov, E. V. Rybak-Akimova, *Chem. Rev.* **2005**, *105*, 2175–2226.
[26] M. H. Lim, J.-U. Rohde, A. Stubna, M. R. Bukowski, M. H. Costas, R. Y. N. , E. Münck, W. Nam, J. Que, *Proc. Nat. Acad. Sci. USA* **2003**, *100*, 3665–3670.
[27] J.-U. Rohde, J.-H. In, M. H. Lim, W. W. Brennessel, M. R. Bukowski, A. Stubna, E. Münck, W. Nam, J. Que, *Science* **2003**, *299*, 1037–1039.
[28] J. Que, *J. Biol. Inorg. Chem.* **2004**, *9*, 684–690.
[29] J. Paschke, M. Kirsch, H.-G. Korth, H. de Groot, R. Sustmann, *J. Am. Chem. Soc.* **2001**, *123*, 11099–11100.
[30] R. Sustmann, H.-G. Korth, D. Kobus, J. Paschke, H. Seiffert, E. Verheggen, E. Bill, M. Kirsch, H. de Groot, unpublished results.
[31] X. Wang, S. Li, Y. Jiang, S, *Inorg. Chem.* **2004**, *43*, 6479–6489.
[32] Earlier calculations[22,23] have shown that the tyrosinate ligand is essential for the mechanistic description of catalase. The calculations predicted that if Compound I is modeled with a bare axial phenolate ligand (as a model for tyrosinate), the latter will be oxidized to the phenoxyl radical. The unpaired spin density of this radical resides largely on the proximal ligand and gives rise to antiferromagnetic coupling with the unpaired spins on the FeO moiety. However, inclusion of a guanidinium ion (as a model for arginine) hydrogen-bonded to phenolate (tyrosinate) led to transfer of the unpaired spin to the porphyrin ligand and ferromagnetic coupling, in agreement with experimental observation.[11] Exploratory calculations (data not shown) revealed that the same is true for our complex. Hence, the proximal hydroxyl ligand serves as a good model for tyrosinate plus arginine.
[33] N. N. Greenwood, A. Earnshaw, *Chemistry of the Elements*, Pergamon Press, Oxford, **1984**, p. 1265.
[34] R. Panicucci, T. C. Bruice, *J. Am. Chem. Soc.* **1990**, *112*, 6063–6071.
[35] S. M. Nelson in *Comprehensive Coordination Chemistry, Vol. 4*, (Ed: G. Wilkinson), Pergamon Press, Oxford, **1987**, Chap. 44.2, pp. 217–276.
[36] F. A. Walker, *Inorg. Chem.* **2003**, *42*, 4526–4544.
[37] T. Sakai, Y. Ohgo, T. Ikeue, M. Takahashi, M. Takeda, M. Nakamura, *J. Am. Chem. Soc.* **2003**, *125*, 13028–13029.
[38] H. Keutel, I. Käpplinger, E.-G. Jäger, M. Grodzicki, V. Schünemann, A. X. Trautwein, *Inorg. Chem.* **1999**, *38*, 2320–22327.

[39] T. Ikeue, T. Saitoh, T. Yamaguchi, Y. Ohgo, M. Nakamura, M. Takahashi, M. Takeda, *Chem. Commun.* **2000**, 1989–1990.
[40] K. L. Kostka, B. G. Fox, M. P. Hendrich, T. J. Collins, C. E. F. Rickard, L. J. Wright, E. Münck, *J. Am. Chem. Soc.* **1993**, *115*, 6746–6757.
[41] K. Meyer, E. Bill, B. Mienert, T. Weyhermüller, K. Wieghardt, *J. Am. Chem. Soc.* **1999**, *121*, 4659–4876.
[42] R. Weiss, A. Gold, J. Terner, *Chem. Rev.* **2006**, *106*, 2550–2579.
[43] Gaussian 03, M. J. Frisch, G. W. Trucks, H. B. Schlegel, G. E. Scuseria, M. A. Robb, J. R. Cheeseman, J. A. J. Montgomery, T. Vreven, K. N. Kudin, J. C. Burant, J. M. Millam, S. S. Iyengar, J. Tomasi, V. Barone, B. Mennucci, M. Cossi, G. Scalmani, N. Rega, G. A. Petersson, H. Nakatsuji, M. Hada, M. Ehara, K. Toyota, R. Fukuda, J. Hasegawa, M. Ishida, T. Nakajima, Y. Honda, O. Kitao, H. Nakai, M. Klene, X. Li, J. E. Knox, H. P. Hratchian, J. B. Cross, C. Adamo, J. Jaramillo, R. Gomperts, R. E. Stratmann, O. C. Yazyev, A. J. Austin, R. Cammi, C. Pomelli, J. W. Ochterski, P. Y. Ayala, K. Morokuma, G. A. Voth, P. Salvador, J. J. Dannenberg, V. G. Zakrzewski, S. Dapprich, A. D. Daniels, M. C. Strain, O. Farkas, D. K. Malick, A. D. Rabuck, K. Raghavachari, J. B. Foresman, J. V. Ortiz, Q. Cui, A. G. Baboul, S. Clifford, J. Cioslowski, B. Stefanov, G. Liu, A. Liashenko, P. Piskorz, I. Komaromi, R. L. Martin, D. J. Fox, T. Keith, M. A. Al-Laham, C. Y. Peng, A. Nanayakkara, M. Challacombe, P. M. W. Gill, B. Johnson, W. Chen, M. W. Wong, C. Gonzalez, J. A. Pople, Gaussian, Inc., Wallingford, CT, **2004**.
[44] J. A. Montgomery, M. J. Frisch, J. W. Ochterski, G. A. Petersson, *J. Chem. Phys.* **1999**, *110*, 2822–2827.
[45] S. P. De Visser, F. Ogliaro, Z. Gross, S. Shaik, *Chem. Eur. J.* **2001**, *7*, 4954–4960.
[46] J. M. Berg, L. Stryer, J. L. Tymoczko, *Biochemie*, Spektrum Akademischer Verlag, Heidelberg, **2003**, pp. 297–298.
[47] W. R. Melik-Adamyan, J. Bravo, X. Carpena, J. Switala, M. J. Mate, I. Fita, P. C. Loewen, *Proteins Struct. Funct. Genet.* **2001**, *44*, 270–281.
[48] V. Guallar, R. A. Friesner, *J. Am. Chem. Soc.* **2004**, *126*, 8501–8508.
[49] R.-J. Cheng, P.-Y. Chen, T. Lovell, T. Liu, L. Noodleman, D. A. Case, *J. Am. Chem. Soc.* **2003**, *125*, 6774–6783.
[50] M. C. Weiss, B. Bursten, S.-H. Peng, V. L. Goedken, *J. Am. Chem. Soc.* **1976**, *98*, 8021–8031.
[51] G. Pelz, K. M. T. Yamada, G. Winnewisser, *J. Mol. Spectrosc.* **1993**, *159*, 507–520.
[52] R. D. Bach, O. Dmitrenko, *J. Am. Chem. Soc.* **2006**, *128*, 1474–1488.
[53] P. K. Sharma, R. Kevorkiants, S. P. de Visser, D. Kumar, S. Shaik, *Angew. Chem.* **2004**, *116*, 1149–1152; *Angew. Chem. Int. Ed.* **2004**, *43*, 1129–1132.
[54] D. Kumar, S. P. de Visser, S. Shaik, *J. Am. Chem. Soc.* **2005**, *127*, 8204–8213.
[55] E. L. Raven, *Nat. Prod. Rep.* **2003**, *20*, 367–381.
[56] S. Kato, T. Ueno, S. Fukuzumi, Y. Watanabe, *J. Biol. Chem.* **2004**, *279*, 52376–52381.
[57] H.-G. Korth, M. I. de Herr, P. Mulder, *J. Phys. Chem. A* **2002**, *106*, 8779–8789.
[58] S. Shaik, S. P. de Visser, F. Ogliaro, H. Schwarz, D. Schröder, *Curr. Opin. Chem. Biol.* **2002**, *6*, 556–567.
[59] A. Decker, E. I. Solomon, *Angew. Chem.* **2005**, *117*, 2292–2295; *Angew. Chem. Int. Ed.* **2005**, *44*, 2252–2255.
[60] NIST Chemistry WebBook, NIST Standard Reference Database Number 69, Gaithersburg MD, 20899, March **2003** (http://webbook.nist.gov).
[61] R. H. Hunt, R. A. Leacock, C. W. Peters, K. T. Hecht, *J. Chem. Phys.* **1965**, *42*, 1931–1946.
[62] M. Kuhn, T. R. Rizzo, D. Luckhaus, M. Quack, M. A. Suhm, *J. Chem. Phys.* **1999**, *111*, 2565–2587.
[63] J. Koput, *J. Mol. Spectrosc.* **1986**, *115*, 438–441.
[64] J.-M. Flaud, C. Camy-Peyret, J. W. C. Johns, B. Carli, *J. Chem. Phys.* **1989**, *91*, 1504–1510.
[65] P. R. Ortiz de Montellano, *Acc. Chem. Res.* **1998**, *31*, 543–549.

Received: August 21, 2006
Revised: December 24, 2006
Published online: February 26, 2007

